Radio emission from merging galaxy clusters : characterizing shocks, magnetic fields and particle acceleration

Weeren, R.J. van

CHAPTER 3

Diffuse steep-spectrum sources from the 74 MHz VLSS survey

Abstract. Galaxy clusters grow by a sequence of mergers with other clusters and galaxy groups. During these mergers, shocks and/or turbulence are created within the intracluster medium (ICM). In this process, particles could be accelerated to highly relativistic energies. The synchrotron radiation from these particles is observed in the form of radio relics and halos that are generally characterized by a steep radio spectral index. Shocks can also revive fossil radio plasma from a previous episode of AGN activity, creating a so-called radio "phoenix". Here we present multi-frequency radio observations of diffuse steep-spectrum radio sources selected from the 74 MHz VLSS survey. Previous Giant Metrewave Radio Telescope (GMRT) observations showed that some of these sources had filamentary and elongated morphologies, which are expected for radio relics. We attempt to understand the nature of diffuse steep-spectrum radio sources and characterize their spectral index and polarization properties. We carried out radio continuum observations at 325 MHz with the GMRT. Observations with the Very Large Array (VLA) and Westerbork Synthesis Radio Telescope (WSRT) were taken at 1.4 GHz in full polarization mode. Optical images around the radio sources were taken with the William Herschel and Isaac Newton Telescope (WHT, INT). Most of the sources in our sample consist of old radio plasma from AGNs located in small galaxy clusters. The sources can be classified as AGN relics or radio phoenices. The spectral indices across most of the radio sources display large variations. We conclude that diffuse steep-spectrum radio sources are not only found in massive X-ray luminous galaxy clusters but also in smaller systems. Future low-frequency surveys will uncover large numbers of steep-spectrum radio relics related to previous episodes of AGN activity.

R. J. van Weeren, H. J. A. Röttgering, and M. Brüggen
Astronomy & Astrophysics, **527**, 114, 2011

3.1 Introduction

Studies of large-scale structure formation show that galaxy clusters grow through mergers with other clusters and galaxy groups, as well as through the continuous accretion of gas from the intergalactic medium (IGM). The baryonic content of clusters is mostly in the form of hot thermal gas visible at X-ray wavelengths. Several clusters also have a non-thermal component within the ICM, which is observable at radio wavelengths (e.g., Ferrari et al. 2008; Giovannini et al. 2009; Giovannini & Feretti 2000; van Weeren et al. 2010). The idea is that shocks and/or turbulence generated during cluster merger events can accelerate particles to relativistic energies, and in the presence of a magnetic field, synchrotron radiation is emitted (e.g., Ensslin et al. 1998; Miniati et al. 2001; Hoeft & Brüggen 2007; Hoeft et al. 2008; Pfrommer 2008; Battaglia et al. 2009; Skillman et al. 2011). These radio sources, which trace the non-thermal component of the ICM, can be divided into several classes.

Radio *halos* are found at the center of merging galaxy clusters and have typical sizes of about a Mpc. They follow the X-ray emission from the thermal ICM and are mostly unpolarized, although there are some exceptions (see Govoni et al. 2005; Bonafede et al. 2009a). Radio halos have been explained by turbulence injected by recent merger events. This injected turbulence might be capable of re-accelerating relativistic particles (e.g., Brunetti et al. 2001; Petrosian 2001). Alternatively, the energetic electrons are secondary products of proton-proton collisions (e.g., Dennison 1980; Blasi & Colafrancesco 1999; Dolag & Enßlin 2000). The turbulent re-acceleration model currently seems to provide a better explanation of the occurrence of radio halos (e.g., Brunetti et al. 2008).

Mini-halos (also called core-halo systems) are diffuse radio sources with sizes $\lesssim$ 500 kpc located in relaxed galaxy clusters, in which diffuse emission surrounds the central cluster galaxy (Murgia et al. 2009; Govoni et al. 2009; Gitti et al. 2007, 2004; Bacchi et al. 2003; Gitti et al. 2002; Burns et al. 1992).

Radio *relics* are irregularly shaped radio sources with sizes ranging from 50 kpc to 2 Mpc, which can be divided into three groups (Kempner et al. 2004). *Radio gischt* are large elongated, often Mpc-sized, radio sources located at the periphery of merging clusters. They probably trace shock fronts in which particles are accelerated via the diffusive shock acceleration mechanism (DSA; Krymskii 1977; Axford et al. 1977; Bell 1978a,b; Blandford & Ostriker 1978; Drury 1983; Blandford & Eichler 1987; Jones & Ellison 1991; Malkov & O'C Drury 2001). Among these are rare double-relics that have two relics located on both sides of the cluster center (e.g., Bonafede et al. 2009b; van Weeren et al. 2009b; Venturi et al. 2007; Bagchi et al. 2006; Röttgering et al. 1997; van Weeren et al. 2010; Brown et al. 2011). According to DSA theory, the integrated radio spectrum should be a single power-law. *Radio phoenices* and *AGN relics* are both related to radio galaxies. AGN relics are associated with extinct or dying radio galaxies. The radio plasma has a steep curved spectrum due to synchrotron and inverse Compton (IC) losses. Fossil radio plasma from a previous episode of AGN activity can also be compressed by a merger shock wave producing a radio phoenix (Enßlin & Gopal-Krishna 2001; Enßlin & Brüggen 2002), these sources again having steeply curved radio spectra. Proposed examples of these are those found by Slee et al. (2001).

In van Weeren et al. (2009c), we presented observations of a sample of 26 diffuse steep-spectrum sources, with $\alpha \leq -1.15$, selected from the 1.4 GHz NVSS (Condon et al. 1998) and 74 MHz VLSS (Cohen et al. 2007) surveys. These sources were either resolved out in the VLA B-array 1.4 GHz snapshot observations or 1.4 GHz FIRST survey (Becker et al. 1995).

GMRT 610 MHz observations of these 26 sources detected one distant powerful radio halo with a radio relic (van Weeren et al. 2009d), five radio relics including two radio phoenices, and one possible mini-halo. The remaining sources were classified as radio sources directly related to AGN activity. The spectral indices of the radio relics in the sample are generally steeper than most previously known relics. By complementing our observations with results for other relics from the literature, we found that the larger relics generally have flatter spectra and are located farther away from the cluster center. This is in line with predictions from shock statistics derived from cosmological simulations (Hoeft et al. 2008; Skillman et al. 2008; Battaglia et al. 2009). In these simulations, it is found that larger shock waves occur mainly in lower-density regions and have larger Mach numbers, and consequently shallower spectra. On the other hand, smaller shock waves are more likely to be found in cluster centers and have lower Mach numbers, thus steeper spectra.

In this paper, we present follow-up radio observations of six sources (i.e., those most likely related to radio relics and halos) found in van Weeren et al. (2009c). GMRT 325 MHz as well as VLA and WSRT 1.4 GHz observations were obtained to create spectral index and polarization maps. Optical images were acquired with the 4.2m WHT and 2.5m INT telescopes at the position of the radio sources to search for optical counterparts and identify galaxy clusters associated with the radio sources.

The layout of this paper is as follows. In Sect. 3.2, we present an overview of the observations and data reduction. In Sect. 3.3, we present the radio and spectral maps as well as optical images around the radio sources. In Sect. 3.4, we show additional optical images around five slightly more compact radio sources (also from the sample of 26 sources) to search for optical counterparts. These sources are not located in nearby galaxy clusters and their nature remains unclear. We end with a discussion and conclusions in Sects. 3.5 and 3.6.

Throughout this paper, we assume a ΛCDM cosmology with $H_0 = 71$ km s^{-1} Mpc^{-1}, $\Omega_m = 0.3$, and $\Omega_\Lambda = 0.7$. All images are in the J2000 coordinate system.

3.2 Observations & data reduction

3.2.1 GMRT 325 MHz observations

Radio continuum observations with the GMRT at 325 MHz were carried out on 14, 15, and 17 May, 2009. Both upper (USB) and lower (LSB) sidebands (IFs, which included RR and LL polarizations) were recorded with a total bandwidth of 32 MHz. The observations were carried out in spectral line mode with 128 channels per IF to facilitate the removal of radio frequency interference (RFI) and reduce the effect of bandwidth smearing. The integration time per visibility was 8 sec. Each source was observed for about 4 hrs in total. The data were reduced with the NRAO Astronomical Image Processing System (AIPS) package.

The data was visually inspected for the presence of RFI, which was subsequently removed (i.e., "flagged"). We carried out an amplitude and phase calibration on the flux and bandpass calibrators 3C147 and 3C286 on a timescale of 8 sec. For this, we chose three neighboring frequency channels free of RFI. These gain solutions were applied before determining the bandpass response of the antennas. This assures that any amplitude and/or phase variations during the scans on the calibrators are corrected before determining the bandpass solutions. At higher frequencies (e.g., 1.4 GHz), both amplitude and phases are assumed to be constant during bandpass calibration. However, for the GMRT observing at low frequencies, this assumption is not

Table 3.1: GMRT 325 MHz observations

	rms noise μJy beam^{-1}	beam size arcsec
VLSS J1431.8+1331	178	$11.8'' \times 7.8''$
VLSS J1133.7+2324	132	$10.4'' \times 7.7''$
Abell 2048	248	$9.7'' \times 9.6''$
24P73	162	$13.6'' \times 9.0''$
VLSS J0004.9−3457	309	$13.5'' \times 11.0''$
VLSS J0915.7+2511	412	$14.7'' \times 8.1''$

always valid and can affect the quality of the bandpass solutions as well as the determination of the flux scale.

After correcting for the bandpass response, both the amplitude and phase solutions for both primary and secondary calibrators were determined but in this case using the full channel range. The fluxes of the primary calibrators were set according to the Perley & Taylor (1999) extension to the Baars et al. (1977) scale. The flux densities for the secondary calibrators were bootstrapped from the primary calibrators. The amplitude and phase solutions were interpolated and applied to the target sources. Some targets were observed over multiple days (observing runs), the resulting different data sets were combined with the AIPS task 'DBCON'.

For each of the target sources, we created a model of the surrounding field using the NVSS survey with a spectral index scaling of −0.7. We carried out a phase-only self-calibration against this model to improve the astrometric accuracy. This was followed by several rounds of phase self-calibration and two final rounds of amplitude and phase self-calibration. To produce the images, we used the polyhedron method (Perley 1989; Cornwell & Perley 1992) to minimize the effects of non-coplanar baselines. The model was then subtracted from the data, a step that facilitated the removal of additional RFI or baselines with problems. Final images were made using robust weighting (robust = 0.5, Briggs 1995). Images were cleaned using the automatic clean-box windowing algorithm in AIPS and cleaned down to 2 times the rms noise level ($2\sigma_{\rm rms}$) within the clean boxes. The final images were corrected for the primary beam response[1]. The uncertainty in the calibration of the absolute flux-scale is in the range $5-10\%$, see Chandra et al. (2004). The resulting noise levels and beam sizes are shown in Table 3.1.

Radio observations at 610 MHz were taken with the GMRT in February and November 2008 of the sources in Table 3.1. The reduction of these observations is similar to the GMRT 325 MHz data and is described in more detail in van Weeren et al. (2009c). We used these images to create the spectral index maps.

3.2.2 VLA 1.4 GHz observations

We carried out L-band observations of four sources with the VLA (see Table 3.2). The observations were taken in standard continuum mode with two IFs, each having a bandwidth of 50 MHz recording all polarization products (RR, LL, RL, and LR). Gain solutions were determined for the calibrator sources and transferred to the target sources. The fluxes for the primary calibrators

[1] http://gmrt.ncra.tifr.res.in/gmrt_hpage/Users/doc/manual/UsersManual/node27.html

Table 3.2: VLA 1.4 GHz observations

	VLSS J1133.7+2324	MaxBCG J217.95869+13.53470	VLSS J0004.9−3457	Abell 2048
Frequency bands (IFs)	1385, 1465 MHz	1385, 1465 MHz	1385, 1465 MHz	1385, 1465 MHz
Bandwidth	2×50 MHz	2×50 MHz	2×50 MHz	2×50 MHz
Polarization	RR, LL, RL, LR	RR, LL, RL, LR	RR, LL, RL, LR	RR, LL, RL, LR
Observation dates	4 Nov 2008, 17 Apr 2009, 10 Aug 2009	2 Nov 2008, 18 Apr 2009, 31 Jul 2009	11 Jun 2009	15 Jul 2009
Project code	AV305, AV312	AV305, AV312	AV312	AV312
Integration time	3.3 s	3.3 s	3.3 s	3.3 s
Total on-source time	5.0 hr, 6.8 hr, 3.9 hr	4.9 hr, 6.8 hr, 3.9 hr	4.0 hr	4.0 hr
VLA configuration	A+B+C	A+B+C	CnB	C
Beam size	$1.3'' \times 1.4''^{a}$, $6.7'' \times 6.7''^{b}$	$1.6'' \times 1.5''^{a}$, $6.4'' \times 5.3''^{b}$	$19.8'' \times 10.3''$	$13.0'' \times 12.4''$
Rms noise ($\sigma_{\rm rms}$)	14^{a}, 19^{b} μJy beam^{-1}	15^{a}, 17^{b} μJy beam^{-1}	49 μJy beam^{-1}	88 μJy beam^{-1}

[a] Briggs weighting (robust = −1.0)
[b] natural weighting

Table 3.3: WSRT observations

Frequency bands 21 cm (IFs)	1311, 1330, 1350, 1370, 1392, 1410, 1432, 1450 MHz
Frequency bands 18 cm (IFs)	1650, 1668, 1686, 1704, 1722, 1740, 1758, 1776 MHz
Bandwidth per IF	20 MHz
Number of channels per IF	64
Channel width	312.5 kHz
Polarization	XX, YY, XY, XY
Observation dates	11, 17, and 18 March, 2009
Integration time	30 s
Total on-source time	6.5 hr 21cm + 6.5 hr 18cm
Beam size	$19.0'' \times 16.5''$
Rms noise ($\sigma_{\rm rms}$)	37 μJy beam^{-1}

were set according to the Perley & Taylor (1999) extension to the Baars et al. (1977) scale. The effective feed polarization parameters (the leakage terms or D-terms) were found by observing the phase calibrator over a wide range of parallactic angles and simultaneously solving for the unknown polarization properties of the source. The polarization angles were set using the polarized sources 3C286 and 3C138. For the R-L phase difference, we assumed values of −66.0 and 15.0 deg for 3C286 and 3C138, respectively. Stokes Q and U images were compiled for each source. From the Stokes Q and U images, the polarization angles (Ψ) were determined ($\Psi = \frac{1}{2}\arctan(U/Q)$). Total polarized intensity (P) images were also made ($P = \sqrt{Q^2 + U^2}$). The polarization fraction were found by dividing the total polarized intensity by the total intensity (Stokes I) image ($\sqrt{Q^2 + U^2}$/I).

3.2.3 WSRT 1.3 – 1.7 GHz observations of 24P73

WSRT observations were taken of a single source (24P73) not included in the VLA observations. Every 5 min, the frequency setup was changed within the L-band, alternating between the 21cm and 18cm setups. Both of these frequency setups have 160 MHz bandwidth divided over 8 IFs, each having 20 MHz bandwidth. The data were recorded in spectral line mode with 64 spectral channels per IF in 4 polarizations. The observations were carried out in three runs on 11, 17, and 18 March, 2009 resulting in a more or less complete 12-hour synthesis run, see Table 3.3.

The data were partly calibrated using the CASA (formerly AIPS++)[2] package. The L-band receivers of the WSRT telescopes have linearly polarized feeds[3]. The leakage terms (D-terms) for the WSRT are frequency dependent (e.g., Brentjens 2008). As a first step, we flagged the autocorrelations, and removed any obvious RFI and corrupted data. Time ranges of antennas affected by shadowing were also taken out. Bandpass and gain solutions were determined using observations of two standard calibrators, both at the start and end of an observing run. The fluxes for the calibrators were set according to the Perley & Taylor (1999) extension to the Baars et al. (1977) scale. We used both polarized (3C138 or 3C286) and unpolarized (CTD93,

[2] http://casa.nrao.edu/

[3] The WSRT records XX = I – Q, YY = I – Q, XY = −U + iV, and XY = −U – iV, where I, Q, U, and V are the Stokes parameters.

3C48) calibrator sources. The bandpass and gain solutions were applied and the data were calibrated for the leakage terms using the unpolarized calibrator source. The polarization angles were set using the polarized calibrators sources, the angles being the same as in Sect. 3.2.2. The data was then exported into AIPS for two rounds of phase only and two rounds of amplitude and phase self-calibration (separately for each IF). The solutions for the amplitude and phase self-calibrations were determined by combing both XX and YY polarizations as Stokes Q is not necessarily zero.

The images for each IF were cleaned to about $2\sigma_{\rm rms}$ using clean boxes. The images for each IF were combined into a deep image by convolving the images of the individuals IFs to a common resolution and using a spectral index scaling of -1.

3.2.4 Optical WHT & INT imaging

Optical images around the radio sources were made using the PFIP camera on the 4.2m WHT telescope and the WFC camera on the INT. The observations were carried out between 15 and 19 April, 2009 (WHT) and 1 – 8 October, 2009 (INT). The field of view was $16' \times 16'$ for the PFIP and $34' \times 34'$ for the WFC camera. The seeing varied between $0.6''$ and $2.0''$, but was mostly between $1.0''$ and $1.5''$. Most nights were photometric. The total integration time per target was about 1500 s for both V, R, and I bands for the WHT observations and 4000 s for the INT observations. The data were reduced with IRAF (Tody 1986, 1993) and the *mscred* package (Valdes 1998). All images were flat-fielded and bias-corrected. The I and R band images were fringe corrected. The individual exposures were averaged, with pixels being rejected above $3.0\sigma_{\rm rms}$ to remove cosmic rays and other artifacts.

Zero-points were determined using various observations of standard stars taken during the nights. Images taken on non-photometric nights were scaled such that the flux of a few targets within the field of view agreed with that of the images taken on photometric nights.

3.3 Results

A list of the observed sources with their integrated fluxes and redshifts is given in Table 3.4. For sources without a spectroscopic redshift, we used the Hubble-K or Hubble-R relations to estimate the redshift (Willott et al. 2003; Snellen et al. 1996; de Vries et al. 2007). Spectral index maps were also made for the radio sources. Only common UV-ranges were used to minimize errors due to differences in the UV-coverage and the individual maps were convolved to the same resolution. For sources with high-resolution ($\lesssim 10''$) 1.4 GHz observations, we created a high-resolution spectral index map between 610 and 1425 MHz. A low-frequency spectral index map between 325 and 610 MHz was also made for most sources. Pixels below $4\sigma_{\rm rms}$ at either one of the two frequency maps were blanked. Low-resolution spectral index maps between 325, 610, and 1425 MHz were created to map the spectral index in low signal-to-noise ratio (SNR) regions. We fitted a single (power-law) spectral index through the three frequencies, pixels below $2.5\sigma_{\rm rms}$ being neglected.

For two sources, the SNR was high enough to create spectral curvature maps. The spectral curvature we defined as $\alpha_{325-610} - \alpha_{610-1425}$. Pixels with a spectral index error larger than 0.06 were blanked in the spectral curvature maps. The errors in the spectral index map are based on the noise levels (rms) of the individual images. In the following subsections, the radio and

spectral index maps are presented together with optical overlays.

3.3.1 VLSS J1133.7+2324, 7C 1131+2341

VLSS J1133.7+2324 is a filamentary radio source, possibly associated with a galaxy cluster at $z = 0.61$ (van Weeren et al. 2009c). To the west of the filamentary source, our 610 MHz image detected diffuse emission associated with the foreground galaxy UGC 6544 located at $z = 0.02385$ (Haynes et al. 1997).

The 325 MHz image (see Fig. 3.1 left panel), is similar to our previous 610 MHz image. In the 325 MHz image, the southern part of the filamentary source is significantly brighter than the northern part, while little emission from UGC 6544 is detected at 325 MHz. The VLA 1.4 GHz image made with natural weighting is shown in Fig. 3.1 (right panel) and reveals much more emission from UGC 6544. The southern part of the filamentary source is quite faint at 1.4 GHz, confirming that it has a steep spectrum. A high-resolution VLA image, also at 1.4 GHz, reveals only three faint compact radio sources, see Fig. 3.3 (left panel). This shows that the emission from the steep-spectrum source is truly diffuse, and cannot be attributed to the combined emission from compact sources. We do not detect any polarized emission from the source at 1425 MHz. We place a 5σ upper limit of 5% on the polarization fraction.

The spectral index map, between 325 and 610 MHz, is shown in Fig. 3.2 (left panel). The spectral index of the southern part of the filamentary source is -2.0, while for the rest of the diffuse emission it is $\alpha \sim -1.7$. Towards UGC 6544, the spectral index flattens. The spectral index map between 610 and 1425 MHz is shown in Fig. 3.2 (right panel). Here the spectral index steepens to $\alpha \leq -2.5$ for the southern part of the filamentary source. The spectral index of the foreground galaxy UGC 6544 is relatively flat with $\alpha \sim -0.5$.

VLSS J1133.7+2324 was also observed by Dwarakanath & Kale (2009) at 1287 MHz with the GMRT and at 330 MHz with the VLA. The reported integrated spectral indices were -1.6 ± 0.03 between 74 and 328 MHz and -1.9 ± 0.08 between 328 and 1278 MHz. The integrated flux density was 151 ± 12 mJy at 328 MHz. We measure a flux of 273 ± 28 mJy at 325 MHz, which is significantly higher than the reported value from Dwarakanath & Kale. This may be partly caused by the higher SNR of our image as we may pick up additional emission beyond what is visible in the Dwarakanath & Kale image. Although, this cannot completely explain the difference in fluxes.

The source could be old radio plasma from a previous episode of AGN activity, although UGC 6544 is a spiral galaxy which normally do not host AGN. If the radio emission were explained by relic lobes, they would be expected to be located symmetrically with respect to the nucleus of the galaxy, which is not the case. The flat spectrum radio emission we detect from the galaxy is fully consistent with that predicted by the far-infrared radio correlation (van Weeren et al. 2009c).

At the location of the filamentary radio source, we detected an overdensity of faint galaxies (see Fig. 3.3). These galaxies are partly hidden behind UGC 6544. The median SDSS photometric redshift is 0.61 for these galaxies. To confirm the presence of a cluster, X-ray observations and/or spectroscopic redshifts of several galaxies are needed.

If this is indeed a distant galaxy cluster, the radio emission is very likely to be associated with the cluster. The source may then trace a shock wave in the cluster where particles are accelerated by the DSA mechanism. In that case the integrated radio spectrum should be a single power-law. Our flux measurements however indicate a slightly curved spectrum. A redshift of 0.61

Table 3.4: Source list & properties

source/cluster	z	S_{325} Jy	S_{1425} mJy	$\alpha_{74-1400}$	curvature $\alpha_{74-610} - \alpha_{610-1425}$	LLS kpc	classification[h]
VLSS J1431.8+1331	0.1599	0.373 ± 0.040	14.6 ± 1.1	-2.03 ± 0.05	1.03[f]	125	AGN + AGNR or PHNX
VLSS J1133.7+2324	0.61 ± 0.16[g]	0.273 ± 0.028	12.3 ± 1.1	-1.69 ± 0.06	0.96	570[g]	AGNR or DSAR
Abell 2048	0.0972	0.559 ± 0.061	18.9 ± 4.3	-1.50 ± 0.05	1.6	310	PHNX
24P73	0.15 ± 0.1[b,g]	0.307 ± 0.033	12.0 ± 3.0	-2.20 ± 0.06	2.0	270	PHNX
VLSS J0004.9−3457	0.3 ± 0.1[e]	0.417 ± 0.046	32.2 ± 1.9	-1.40 ± 0.04	0.30[f]	200	AGN (or MH + DSAR?)
VLSS J0915.7+2511	0.324	0.417 ± 0.046	24.7 ± 1.5[a]	-1.52 ± 0.04	1.02	190	AGNR or PHNX
VLSS J1117.1+7003	0.8 ± 0.4[d]	0.030 ± 0.006[c]	2.9 ± 0.5[a]	-1.87 ± 0.07	0.0	130	AGN?
VLSS J2043.9−1118	0.5 ± 0.3[d]	...	7.7 ± 0.6[a]	-1.74 ± 0.05	0.84	250	AGN (MH? + DSAR?)
VLSS J0516.2+0103	1.2 ± 0.7[d]	...	4.3 ± 0.4[a]	-1.73 ± 0.06	0.0	290	AGN (or MH?)
VLSS J2209.5+1546	1.1 ± 0.7[d]	...	7.0 ± 0.9[a]	-1.56 ± 0.07	0.59	500	AGN?
VLSS J2241.3−1626	0.5 ± 0.3[d]	...	14.6 ± 1.1[a]	-1.44 ± 0.06	0.0	290	AGN?

[a] flux from NVSS (Condon et al. 1998)
[b] identification of the cD galaxy uncertain
[c] flux from WENSS (Rengelink et al. 1997)
[d] redshift estimated using the fitted Hubble-R relation from de Vries et al. (2007), since it is unclear whether there is a common underlying population of massive elliptical galaxies for extended steep-spectrum radio sources we have taken the 3C Hubble-R relation from Snellen et al. (1996) as an upper limit for the redshift (i.e., the 3C galaxies are about 1 mag brighter at the same redshift)
[e] redshift estimated using the fitted Hubble-K relation from Willott et al. (2003)
[f] varies across the source
[g] association with cluster uncertain
[h] PHNX = radio phoenix, AGNR = AGN relic, MH = radio mini-halo, DSAR = relic tracing shock wave with DSA

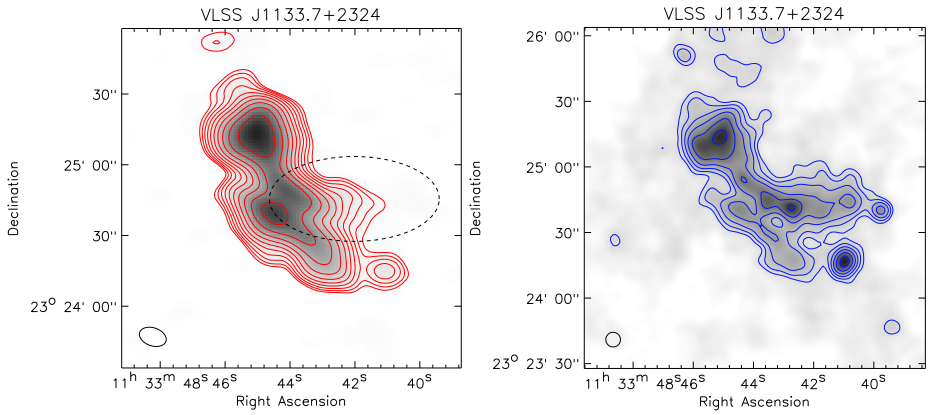

Figure 3.1: Left: GMRT 325 MHz map. Contour levels are drawn at $\sqrt{[1,2,4,8,\ldots]} \times 4\sigma_{\rm rms}$. The position of is UGC 6544 is indicated by the dashed ellipse. Right: VLA 1425 MHz map. Contour levels are drawn as in the left panel.

would correspond to a physical size of about 500 kpc. The very steep and somewhat curved radio spectrum then suggest the source to be an AGN relic, rather than a radio phoenix because the source is quite large and the time to compress such a large radio "ghost" would remove most of the electrons responsible for the radio emission by radiative energy losses (Clarke & Ensslin 2006). Additional flux measurements at lower and/or higher frequencies will be needed to confirm whether the radio spectrum is indeed curved.

3.3.2 VLSS J1431.8+1331, MaxBCG J217.95869+13.53470

VLSS J1431.8+1331 is located in the galaxy cluster MaxBCG J217.95869+13.53470 (z = 0.1599, Koester et al. 2007) and associated with the central cD galaxy of the cluster. The cluster has a moderate X-ray luminosity of $L_{\rm X,\ 0.1-2.4\ keV} \sim 1 \times 10^{44}$ erg s^{-1} based on the ROSAT count rate (Voges et al. 1999). The GMRT 325 MHz image (see top left panel Fig. 3.4) shows a bright elongated source. To the west a somewhat fainter diffuse component can be seen. This component is not associated with any optical galaxy (see Fig. 3.3, right panel). A third fainter source is located further to the southwest. The first two components are connected by a faint radio "bridge". This bridge was not seen in our previous 610 MHz image. The bright source is a currently active radio galaxy with the radio core clearly being visible in our VLA 1.4 GHz images (see Fig. 3.4 top middle and right panels). Probably, radio plasma from the core flows westwards and then forms the north-south elongated structure.

The spectral index maps (see Fig. 3.4 bottom panels), are indicative of a relatively flat spectral index of -0.5 for the radio core between 325 and 610 MHz. Spectral steepening is observed to the north and south of the elongated structure. The spectral index for the southern part of the elongated structure steepens to -3.5 between 610 and 1425 MHz. The spectral index of the southwestern component is about -1.5 between 325 and 610 MHz, there being smaller spectral index variations across it than in the brighter western component. Between 610 and 1425 MHz, the spectral index steepens to about -2.5. The spectral curvature map ($\alpha_{325-610} - \alpha_{610-1425}$) (see

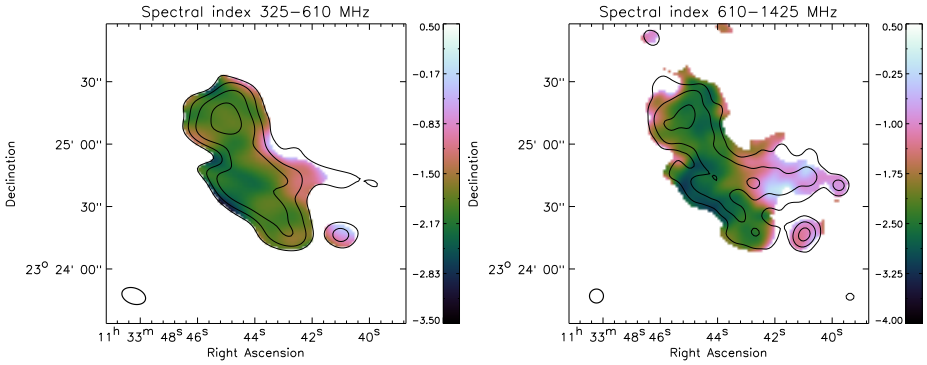

Figure 3.2: Left: Spectral index map between 325 and 610 MHz at a resolution of $11.75'' \times 7.65''$. Contour levels are from the 325 MHz GMRT image and drawn at levels of $[1, 2, 4, 8, \ldots] \times 6\sigma_{\rm rms}$. Right: Spectral index between 610 and 1425 MHz. Contour levels are from the 1425 MHz VLA image and drawn at levels of $[1, 2, 4, 8, \ldots] \times 5\sigma_{\rm rms}$. The beam size is $6.7'' \times 6.7''$.

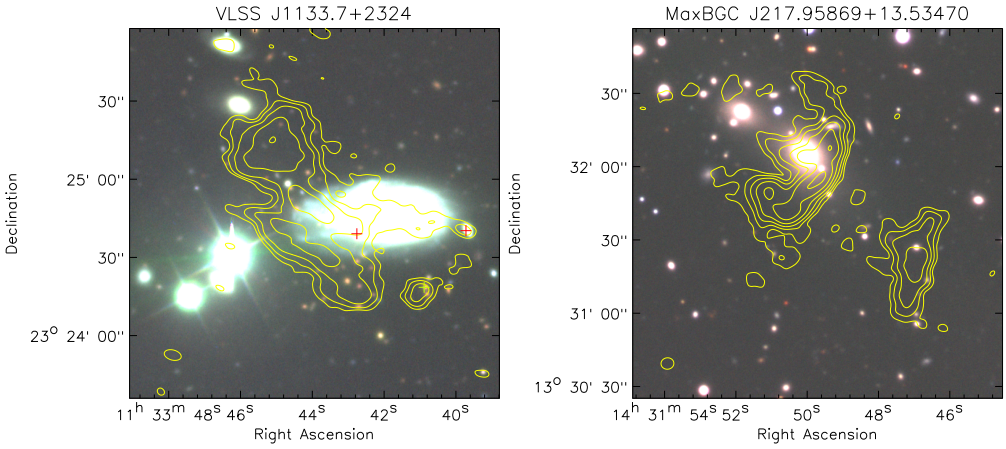

Figure 3.3: Left: Optical WHT color image for VLSS J1133.7+2324. GMRT 610 MHz contours are overlaid. The beam size is $6.6'' \times 3.9''$. Three compact sources detected in the VLA 1425 MHz high-resolution image are marked with crosses. Right: Optical WHT color image for MaxBCG J217.95869+13.53470. GMRT 610 MHz contours are overlaid. The beam size is $5.3'' \times 4.8''$. Contour levels are drawn as in the left panel.

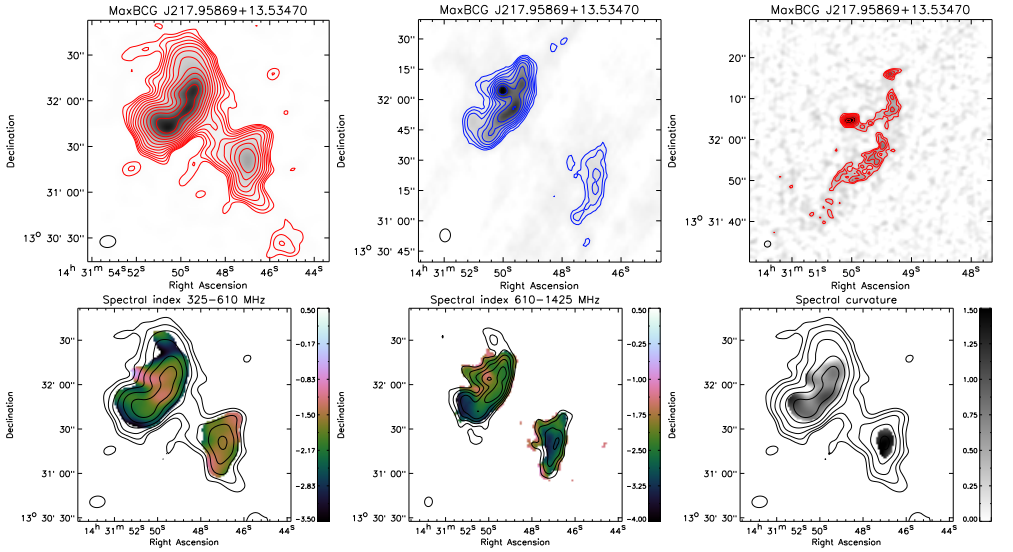

Figure 3.4: Top left: GMRT 325 MHz map. Contour levels are drawn as in Fig. 3.1. Top middle: VLA 1425 MHz map. Contour levels are drawn as in Fig. 3.1. Top right: VLA 1425 MHz high-resolution image. The image was made using Briggs weighting with robust set to −1. Contour levels are drawn at $\sqrt{[1, 2, 4, 8, \ldots]} \times 4\sigma_{\rm rms}$. Bottom left: Spectral index map between 325 and 610 MHz at a resolution of $10.4'' \times 7.7''$. Contour levels are from the 325 MHz GMRT image and drawn at levels of $[1, 2, 4, 8, \ldots] \times 6\sigma_{\rm rms}$. Bottom middle: Spectral index between 610 and 1425 MHz. Contour levels are from the 610 MHz GMRT image and drawn at levels of $[1, 2, 4, 8, \ldots] \times 5\sigma_{\rm rms}$. The beam size is $6.41'' \times 5.26''$. Bottom right: Spectral curvature map. Contour levels are drawn as in the left panel and the resolution is $10.4'' \times 7.7''$.

Fig. 3.4 bottom right panel), shows that the southwestern source has a very curved radio spectrum. The southern end of the radio structure from the active AGN is also quite curved. The high spectral curvature is likely to be the result of spectral ageing, the gradient in the spectral index away from the core providing evidence of this. The two diffuse sources the southwest of the active AGN are probably old "bubbles" of radio plasma linked to this AGN, which is consistent with the curved radio spectrum. The presence of a faint radio bridge also suggests a relation between this southwestern component and the radio galaxy. The southwestern component can therefore be classified as a radio phoenix (if the radio plasma has been compressed) or an AGN relic. XMM-Newton observations of the cluster will be presented by Ogrean et al. (submitted).

3.3.3 VLSS J2217.5+5943, 24P73

This source was discovered during the Synthesis Telescope of the Dominion Radio Observatory (DRAO) Galactic plane survey at 408 MHz and 1.42 GHz (Higgs 1989; Joncas & Higgs 1990). Green & Joncas (1994) found the source to be diffuse and have an ultra-steep spectrum ($\alpha = -2.58 \pm 0.14$). Our GMRT 610 MHz observations (see Fig. 3.5 bottom right panel) detected a very complex filamentary source, resembling the relics found in Abell 13 and Abell 85 (Slee et al. 2001). Our GMRT 325 MHz image, Fig. 3.5 top left panel, is similar to the 610 MHz

image. In our combined WSRT 1.3 − 1.8 GHz image (top right panel), the fainter western part of the relic is only marginally detected, which is indicative of a steep spectral index in this region. We set an upper limit to the polarization fraction of 5% for the source at 1.4 GHz.

The spectral index map between 325 and 610 MHz is shown in the bottom left panel of Fig. 3.5. The spectral index varies between −1.4 and −2.9 over the source. The western part of the source has the steepest spectrum. Towards the southwest, the spectral index flattens to about −1.0. This part may be associated with a separate compact radio AGN.

Our optical WHT image (bottom right panel Fig. 3.5) is dominated by foreground stars as the source is located in the Galactic plane, at Galactic latitude of 2.44 degrees. However, there are also several faint red galaxies seen in the image that may belong to a galaxy cluster, and these are marked by circles. The brightest galaxy (located southwest) has an R-band magnitude of 20.69. Using the Hubble-R relation (de Vries et al. 2007), we estimate a redshift of 0.15 ± 0.1, including an extinction in the R-band of 4.173 mag (Schlegel et al. 1998). We note that this redshift estimate is based on the corrected identification of the cD galaxy in the cluster. If the source is indeed located at $z = 0.15$, then its largest physical extent is 270 kpc. We classify the source as a radio phoenix given the filamentary morphology and extreme spectral index. In fact, the relic is very similar to the proposed phoenix in Abell 13 (Slee et al. 2001). To confirm the presence of a cluster, deep near-infrared (NIR) imaging will be necessary.

3.3.4 VLSS J0004.9−3457

The radio source is located in a small galaxy cluster or group, B02291 (Zanichelli et al. 2001). The cluster/group is located at a redshift of 0.3 ± 0.1 (van Weeren et al. 2009c). No X-ray emission from the system is detected in the ROSAT All-Sky Survey (Voges et al. 1999, 2000), which implies that the system is not very massive. An optical POSS-II color composite is shown in Fig. 3.6 (bottom right panel). The various radio components are labeled alphabetically (see Fig. 3.6 top right panel).

Our GMRT 325 MHz image of VLSS J0004.9−3457 (top left panel) displays a diffuse source (A) centered on a K-mag=14.86 galaxy. The source extends somewhat further northwards than in the 610 MHz image (bottom right panel).

Source B is associated with another galaxy, C does not have an optical counterpart and seems to be related to source A. Source D is a fainter source (resolved in the 610 MHz image) located just east of VLSS J0004.9−3457 at RA $00^{h}\ 04^{m}\ 50^{s}$, Dec $-34^{\circ}\ 56'\ 38''$. In the CnB-array VLA 1.4 GHz image, shown in Fig. 3.6 (top right), component C is less prominent than in the 325 MHz image, while source B is clearly visible.

The spectral index map between 325 and 610 MHz is shown in Fig. 3.7 (right panel). Source B has a flat spectral index of ~ -0.5. Source D has a steeper spectral index of −1.1. The spectral index of A steepens away from the center (defined as the peak flux and located at the position of the K-mag=14.86 galaxy). The central region has a spectral index of −1.2. Outwards, the spectral index steepens to < -2. Component C has a spectral index of about −1.5. A spectral index map, for the frequencies 325, 610, and 1425 MHz, is shown in Fig. 3.7 (middle panel). The spectral curvature map, in the right panel of Fig. 3.7, shows the least curvature (i.e., less than 0.5 units) for the western part of A and source B. Emission to the east of A shows more spectral steepening, with a curvature of about 1.0 units.

Polarized emission from source A, B, and component C is observed in the VLA images, Fig. 3.6 (bottom left panel). Source B is polarized at the 8% level. The polarization fraction at

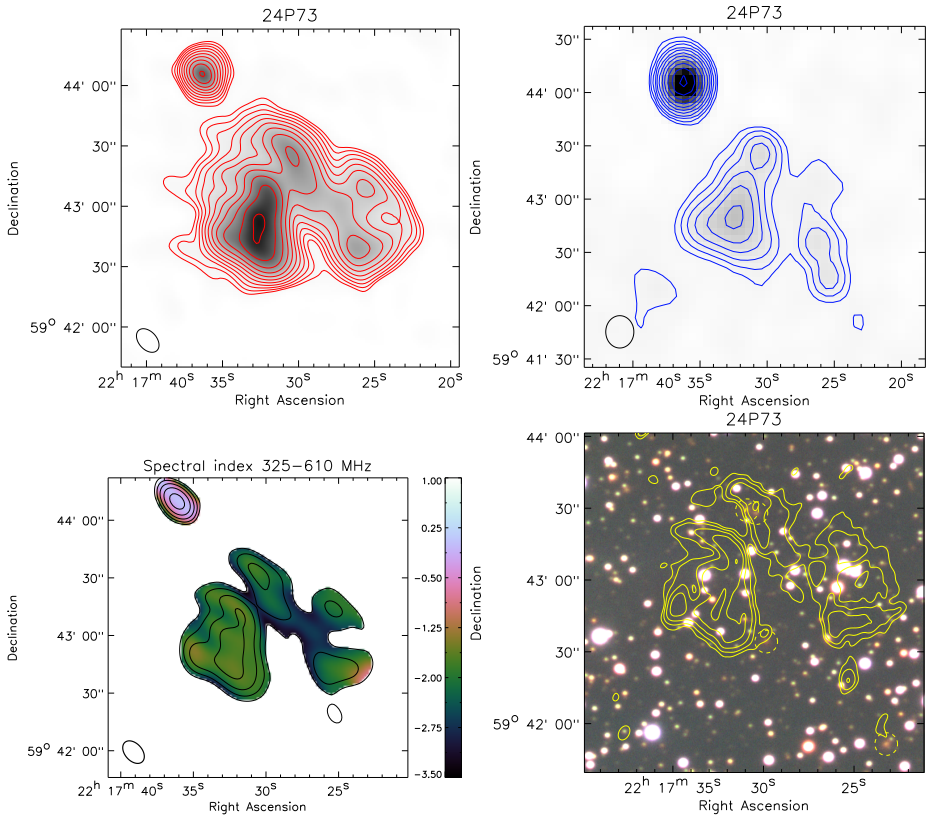

Figure 3.5: Top left: GMRT 325 MHz map. Contour levels are drawn as in Fig. 3.1. Top right: WSRT 1.3 – 1.8 GHz map. Contour levels are drawn as in Fig. 3.1. Bottom left: Spectral index map between 325 and 610 MHz at a resolution of $13.44'' \times 8.96''$. Contour levels are from the 325 MHz image and drawn as in Fig. 3.2. Bottom right: Optical WHT color image for 24P73. GMRT 610 MHz contours are overlaid. The beam size is $6.4'' \times 4.3''$. Contour levels are drawn as in Fig.3.3. Several faint galaxies in the image are marked by circles.

the center of A is roughly 6%. The arc-like southeast extension (C) is highly polarized, with a polarization fraction between 25 and 35%.

We tentatively classify the source as a 200 kpc "mini-halo" (or core-halo), because the radio emission of diffuse source A surrounds a central galaxy in a cluster or galaxy group. The spectral steepening away from the core is then the result of synchrotron and IC losses. The eastern arc-like extension could be a radio relic based on its elongated nature and high polarization fraction. The high polarization fraction is indicative of the presence of ordered magnetic fields. Therefore it is likely that this component traces a region in the ICM that has been compressed by a shock wave. Radio mini-halos usually occur in massive relaxed galaxy clusters. The possible presence of a radio relic indicates merger activity so it is possible that the "mini-halo" can also be linked to the merger activity of the system. Radio plasma from the central AGN might have been re-accelerated or compressed by this merger event. The source is somewhat similar to MRC 0116+111 studied by Gopal-Krishna et al. (2002) and Bagchi et al. (2009). We find that MRC 0116+111 exhibits two bubble-like radio lobes, whereas VLSS J0004.9−3457 seems to consist of a single component. The morphology of the source is more similar to the core-halo system in ZwCl 1454.8+2223 and candidate core-halo system in Abell 3444 (Venturi et al. 2008, 2007). The cluster/group would make an interesting target for future X-ray observations to study the relation between the radio sources and the surrounding ICM.

3.3.5 VLSS J0915.7+2511, MaxBCG J138.91895+25.19876

The radio source is located in the cluster MaxBCG J138.91895+25.19876. The source consists of a northern component (Fig. 3.8 left panel) and a slightly more extended fainter component to the south. A compact source to the west is associated with the galaxy J091539.68+251136.9. This source has a spectroscopic redshift (SDSS DR7, Abazajian et al. 2009) of 0.324. This cluster has a photometric redshift of 0.289 (Koester et al. 2007), but the galaxy seems to be part of the cluster, hence we adopt a redshift of 0.324 for the cluster. The compact source is resolved in our 610 MHz GMRT image and displays a double lobe structure (see Fig.3.8 right panel).

The spectral index map between 325 and 610 MHz is shown in Fig. 3.8 (middle panel). The spectral index map is noisy because of dynamic range limitations from the source 4C +25.24 (1.35 Jy at 325 MHz) located about 3′ to the southeast. The eastern part of the northern component has the steepest spectrum with an index of $\alpha \sim -2$, although the SNR is low in this region. The compact source to the west has a flat spectral index of about −0.2.

The classification of the source is unclear. The source might contain old radio plasma that originated in the AGN to the west. In this case, the source could be classified as a radio phoenix or AGN relic.

3.3.6 VLSS J1515.1+0424, Abell 2048

VLSS J1515.1+0424 is located in the cluster Abell 2048 ($z = 0.0972$; Struble & Rood 1999) to the east of the cluster center. The source has a largest extent of 310 kpc (see Fig. 3.9 top left panel), and has a complex morphology. Only the brighter parts of the source are seen in the VLA 1.4 GHz C-array image (Fig. 3.9 top right panel). No polarized flux is detected from the source. We set an an upper limit on the polarization fraction of 8% for the source, again requiring a SNR of 5 for a detection. An optical V, R, and I color image of the cluster with 610 MHz contours overlaid does not reveal an obvious optical counterpart for the source.

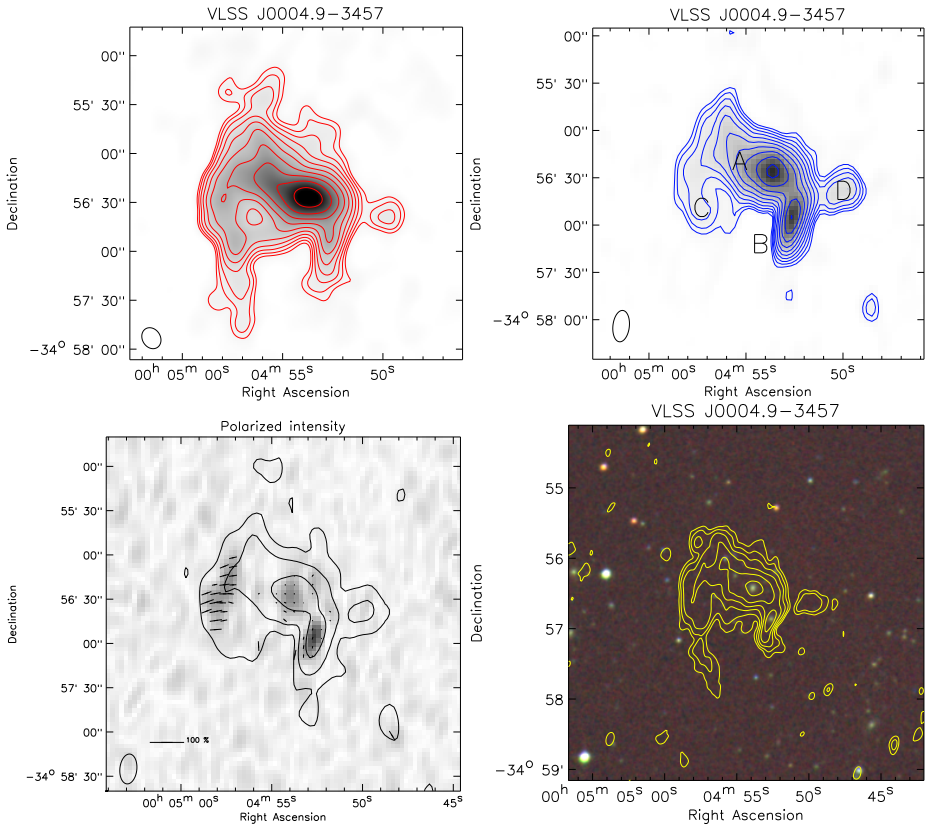

Figure 3.6: Top left: GMRT 325 MHz map. Contour levels are drawn as in Fig. 3.1. Top right: VLA 1425 MHz map. Contour levels are drawn as in Fig. 3.1. Bottom left: VLA 1425 MHz polarization map. Total polarized intensity is shown as grayscale image. Vectors refer to the polarization E-vectors, with their length representing the polarization fraction. A reference vector for a polarization fraction of 100% is shown in the bottom left corner. The polarization fractions were corrected for Ricean bias (Wardle & Kronberg 1974). No polarization E-vectors were drawn for pixels with a SNR less than 3 in the total polarized intensity map. Contours show the total intensity image (Stokes I) at 1425 MHz. Contour levels are drawn at $[1, 16, 256, 4096, \ldots] \times 0.147$ mJy beam^{-1}. Bottom right: Optical POSS-II color image for VLSS J0004.9−3457. GMRT 610 MHz contours are overlaid. The beam size is $6.4'' \times 4.3''$. Contour levels are drawn as in Fig.3.3.

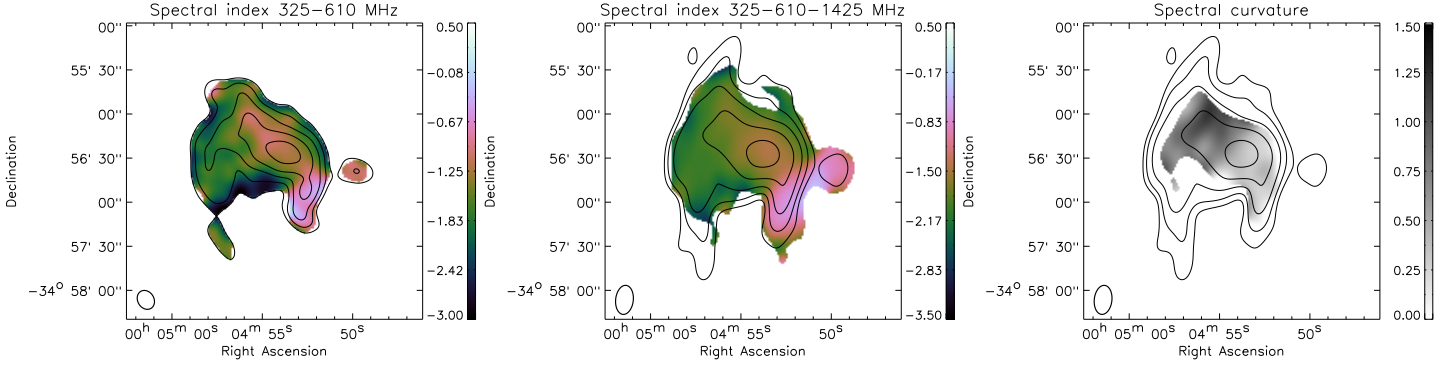

Figure 3.7: Left: Spectral index map between 325 and 610 MHz at a resolution of $13.5'' \times 11.0''$. Contour levels are from the 325 MHz image and drawn as in Fig. 3.2. Middle: Power-law spectral index fit between 325, 610, and 1425 MHz. Contours are from the 325 MHz image and drawn at levels of $[1, 2, 4, 8, \ldots] \times 4\sigma_{\rm rms}$. The beam size is $19.83'' \times 12.0''$. Right: Spectral curvature map. Contour are drawn as in the middle panel.

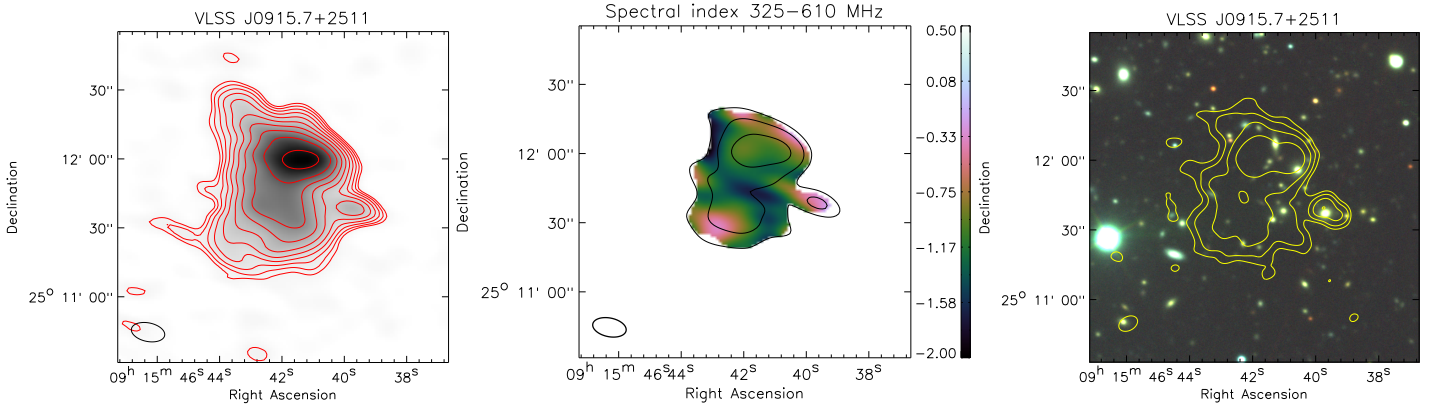

Figure 3.8: Left: GMRT 325 MHz map. Contour levels are drawn as in Fig. 3.1. Middle: Spectral index map between 325 and 610 MHz at a resolution of $14.7'' \times 8.1''$. Contour levels are from the 325 MHz image and drawn as in Fig. 3.2. Right: Optical WHT color image for VLSS J0915.7+2511. GMRT 610 MHz contours are overlaid. The beam size is $8.6'' \times 5.9''$. Contour levels are drawn as in Fig.3.3.

The spectral index map between 325, 610, and 1425 MHz, is shown in Fig. 3.9 (bottom left panel). No systematic spectral index gradients are seen across the source. A region with a flat spectral index ($\alpha > -0.5$) is located under the southern "arm" of the source at RA $15^{\rm h}\ 15^{\rm m}\ 08.6^{\rm s}$, Dec $+04^\circ\ 23'\ 08''$. This part is associated with the galaxy 2MASX J15150860+0423085 in front of the cluster ($z = 0.047856$ from SDSS DR7) (see Fig. 3.9 bottom right panel). The spectral index of the relic is steep with an average value of about -1.7 between 1425 and 325 MHz.

The complex morphology of the radio source suggests that the source can be classified as a radio phoenix. The steep curved radio spectrum is consistent with this interpretation. If the source is indeed a radio phoenix, the radio plasma should have originated in a galaxy that has gone through phases of AGN activity. A candidate is the elliptical galaxy MCG +01−39−011 ($z = 0.095032$; Slinglend et al. 1998). This galaxy is currently active and located close to the eastern end of the southern "arm". However, there are several other elliptical galaxies around, although at the moment they are not radio-loud. A ROSAT image (see van Weeren et al. 2009c) of the cluster shows a substructure to the east of the main cluster, which implies that the cluster is presently undergoing a merger. The velocity dispersion, σ, of the galaxies in the cluster is 857 km s^{-1} (Shen et al. 2008). The bolometric X-ray luminosity is 1.914×10^{44} erg s^{-1}. On the basis of the $L_{\rm X} - \sigma$ relation (X-ray luminosity versus velocity dispersion) from Shen et al.

$$\log\left(\frac{L_X}{10^{44}\ {\rm erg\ s^{-1}}}\right) = 4.39 \log\left(\frac{\sigma}{500\ {\rm km\ s^{-1}}}\right) - 0.530\ , \tag{3.1}$$

we predict a velocity dispersion of 765 ± 40 km s^{-1} given the X-ray luminosity. This is lower than the observed value, which is not inconsistent with the cluster having undergone a recent merger event. A shock wave generated by the proposed merger event might have compressed fossil radio plasma and produced the radio phoenix. Future X-ray observations will be needed to study the dynamical state of the cluster and the relation between the ICM and the radio phoenix.

3.4 Optical imaging around five compact steep-spectrum sources

We present optical images around five slightly more compact steep-spectrum radio sources, which nature was found to be unclear in van Weeren et al. (2009c).

3.4.1 VLSS J2043.9−1118

The radio source has a largest angular size of 41″. An optical counterpart (R band magnitude of 20.1) is visible in our WHT image (see Fig. 3.10). The radio emission surrounds the galaxy and there is a hint of a faint extension to the east. We estimate a redshift of 0.5 ± 0.3 for the optical counterpart, which implies a physical extent of 250 kpc for the radio source. The source could be a mini-halo or core-halo system given its steep spectral index of -1.74 ± 0.05 (between 74 and 1400 MHz). Alternatively, we are detecting radio plasma from an AGN that has undergone a significant amount of spectral ageing.

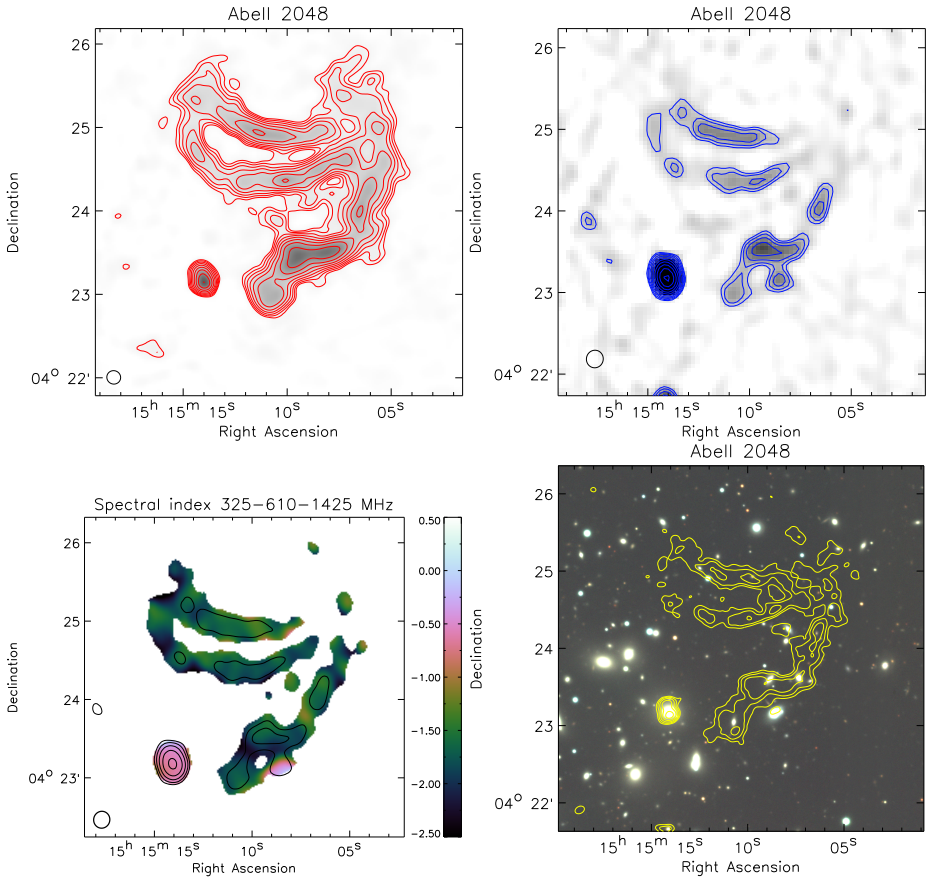

Figure 3.9: Tot left: GMRT 325 MHz map. Contour levels are drawn as in Fig. 3.1. Top right: VLA 1425 MHz map. Contour levels are drawn as in Fig. 3.1. Bottom left: Power-law spectral index fit between 325, 610, and 1425 MHz. Contours are from the 1.4 GHz VLA image and drawn as in Fig. 3.2 (left panel). The resolution is $13.0'' \times 12.4''$. Bottom right: Optical WHT color image for Abell 2048. GMRT 610 MHz contours are overlaid. The beam size is $7.6'' \times 5.4''$. Contour levels are drawn as in Fig.3.3.

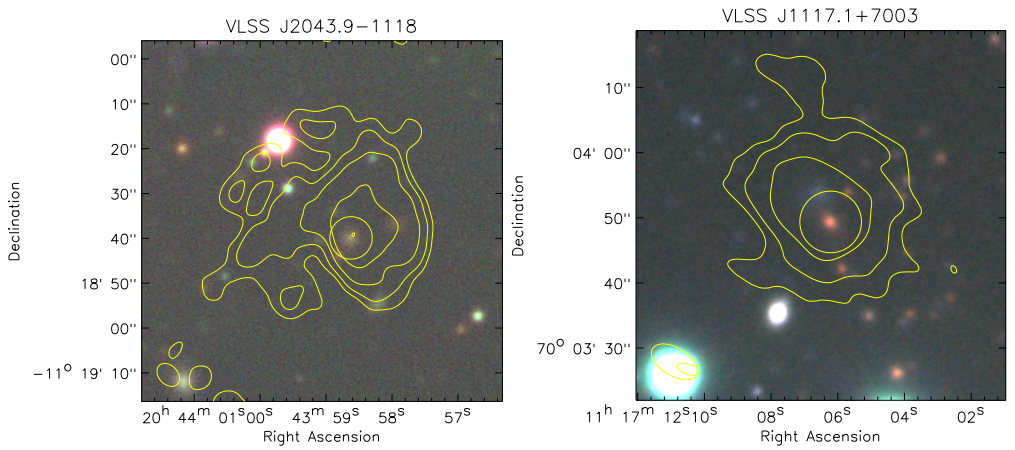

Figure 3.10: Left: Optical WHT color image for VLSS J2043.9−1118. GMRT 610 MHz contours are overlaid. The beam size is 5.8″ × 4.2″. Contour levels are drawn as in Fig.3.3. A circle indicates the proposed optical counterpart. Right: Optical WHT color image for VLSS J1117.1+7003. GMRT 610 MHz contours are overlaid. The beam size is 7.8″ × 4.3″. Contour levels are drawn as in Fig.3.3. A circle indicates the proposed optical counterpart.

3.4.2 VLSS J1117.1+7003

This source has a remarkably steep radio spectrum ($\alpha_{74-1400} = -1.87 \pm 0.07$) without any indication of a spectral turnover at low frequencies. The source is resolved into a smooth featureless roughly spherical blob (26″ by 23″). We identify a red galaxy, with an R magnitude of 21.2, as a possible counterpart, which would put the source at a redshift of 0.8 ± 0.4. A blue galaxy is located only 5″ north of the red galaxy. This might also be the counterpart of the radio source. The integrated R-band magnitude is about the same as the redder galaxy putting it at about the same redshift if it were the optical counterpart. At $z = 0.8$, the radio emission would have a physical extent of 130 kpc.

3.4.3 VLSS J2209.5+1546

The radio map shows an elongated source. We find a faint (R band magnitude of 22.4) counterpart halfway along the elongated source. We estimate a redshift of $z = 1.1 \pm 0.7$ (using the Hubble-R relation), giving a physical extent of 500 kpc.

3.4.4 VLSS J0516.2+0103

VLSS J0516.2+0103 is a slightly elongated source that does not have an optical counterpart in POSS-II images. In our INT image, we identify a possible faint red counterpart with an R magnitude of 22.9. This implies a redshift of 1.2 ± 0.7 (including an extinction of 0.367 in the R band), which gives a size of 290 kpc and makes it a candidate mini-halo or core-halo system.

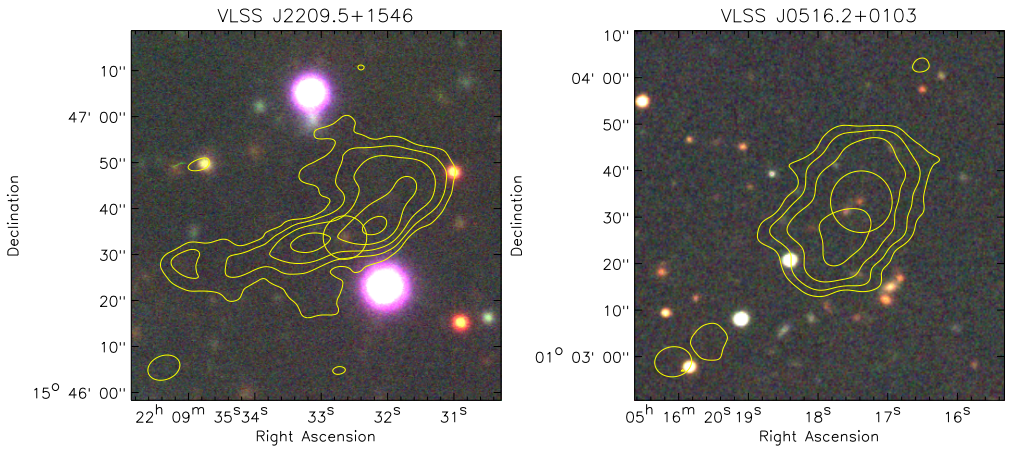

Figure 3.11: Left: Optical WHT color image for VLSS J2209.5+1546. GMRT 610 MHz contours are overlaid. The beam size is $6.9'' \times 6.2''$. Contour levels are drawn as in Fig.3.3. A circle indicates the proposed optical counterpart. Right: Optical INT color image for VLSS J0516.2+0103. GMRT 610 MHz contours are overlaid. The beam size is $8.1'' \times 6.5''$. Contour levels are drawn as in Fig.3.3. A circle indicates the proposed optical counterpart.

3.4.5 VLSS J2241.3−1626

The morphology of this source is complex. A potential optical counterpart has an R-band magnitude of 20.2 giving a redshift of 0.5 ± 0.3 and a physical extent of 290 kpc for the source. The optical counterpart is located roughly halfway along the extended source. The enhancements in the radio emission to the east and west of the proposed counterpart suggest that these are the lobes of an AGN. The fainter more-extended radio emission might be older radio plasma causing the steep radio spectrum.

3.5 Discussion

Most radio relics and halos known till date are located within massive X-ray luminous clusters. The majority of these sources were discovered in the NVSS and WENSS surveys by visual inspection of the radio maps in and around known galaxy clusters (mostly Abell clusters, Giovannini et al. 1999; Kempner & Sarazin 2001). Venturi et al. (2007, 2008) carried out a search in a complete sample of 50 massive X-ray selected ($L_{\mathrm{X,\ 0.1–2.4\ keV}} > 5 \times 10^{44}$ erg s^{-1}) clusters to determine the fraction of radio halos in these systems. The fraction of clusters hosting a giant radio halo was found to be 0.29 ± 0.09. The number of small galaxy clusters with low X-ray luminosity known to host a diffuse radio source is very small. An example is the radio halo in Abell 1213 identified by Giovannini et al. (2009) with $L_{\mathrm{X,\ 0.1–2.4\ keV}} = 0.1 \times 10^{44}$ erg s^{-1}.

We note that the sources presented in this paper were selected on the basis of their steep spectral index and diffuse nature. There was no requirement for the radio sources to be located in a galaxy cluster. The question arises of whether most radio relics and halos are indeed located in massive galaxy clusters or whether they also occur in poor clusters and galaxy groups.

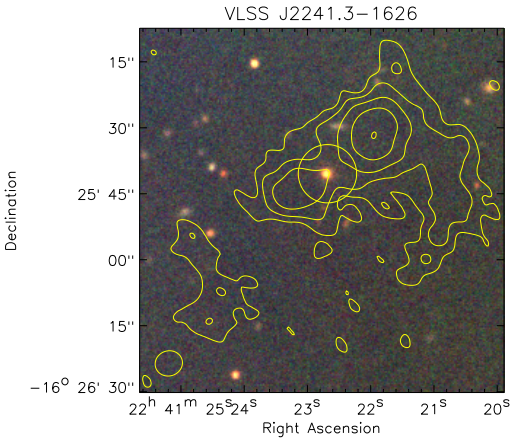

Figure 3.12: Optical INT color image for VLSS J2241.3−1626. GMRT 610 MHz contours are overlaid. The beam size is 6.1″×5.8″. Contour levels are drawn as in Fig.3.3. A circle indicates the proposed optical counterpart.

None of the sources in our sample, with $\alpha < -1.35$ (between 74 and 1400 MHz), are located in massive known galaxy clusters. Only VLSS J1515.1+0424 (in Abell 2048) and VLSS J1431.8+1331 (in MaxBCG J217.95869+13.53470) are found in clusters detected in the ROSAT All-Sky Survey. The X-ray luminosities of these clusters are moderate, with values between 1–2 $\times 10^{44}$ erg s^{-1}. Therefore, our observations indicate that diffuse steep-spectrum sources do also occur in less massive clusters and galaxy groups. Most of the sources seem to be radio relics related to previous episodes of AGN activity: either AGN relics or radio phoenices. Some other sources in our sample can be classified as core-halo or mini-halo candidates, where the radio emission surrounds a central galaxy of a poor cluster or galaxy group. In our case, they are not found in massive cool-core clusters.

Amongst the sources in our sample, there are also a number of more distant ($z \sim 1$) filamentary radio sources related to AGN activity. These could be relatively "nearby" ultra-steep spectrum (USS) sources (e.g., see Miley & De Breuck 2008, for a review). As they are relatively nearby, they are clearly extended in for example the 1.4 GHz FIRST survey images (5″ resolution) and therefore included in our sample.

We did not detect any ultra-steep spectrum radio halos (Brunetti et al. 2008) in our sample. This could be because the surface brightness of these objects is too low for them to be detected in the 74 MHz VLSS survey (Brunetti et al. 2008; Macario et al. 2010). The 74 MHz VLSS survey is relatively shallow with an average rms noise of 0.1 Jy beam^{-1}.

Since poor galaxy clusters and groups are more numerous, it is expected that the sources in our sample are only the tip of the iceberg and many more of them should turn up in low-frequency surveys, as will be carried out for example by LOFAR in the near future. In terms also of the timescales related to AGN activity and the ubiquity of shocks, these surveys will uncover large populations of AGN relics and radio phoenices. One of the difficulties will be to classify these sources on the basis of the radio morphology, polarization, and spectral index alone. The differences between radio phoenices, AGN relics, and relics tracing shock fronts with DSA are

often subtle. The AGN relics and phoenices should have very curved radio spectra, while relics caused by electrons accelerated at shocks should have straight radio spectra. Nevertheless, deep optical/NIR and X-ray surveys will play an important role in identifying the nature of these diffuse radio sources.

3.6 Conclusions

We have presented 325 MHz and 1.4 GHz radio observations of six diffuse steep-spectrum sources. The sources were selected from an initial sample of 26 diffuse steep-spectrum ($\alpha < -1.15$) sources (van Weeren et al. 2009c). Optical WHT and INT images were taken at the positions of 10 radio sources from the sample. We briefly summarize the results.
-The radio source VLSS J1431.8+1331 is located in the cluster MaxBCG J217.95869+13.53470 ($z = 0.16$) and associated with the central cD galaxy. A second radio source is located 175 kpc to the east. This source is connected by a faint radio bridge to the central radio source. This source probably traces an old bubble of radio plasma from a previous episode of AGN activity of the central source. The spectral curvature of this source is large, indicating the radio plasma is old, which is consistent with the above scenario.
-VLSS J1133.7+2324 is an elongated filamentary steep spectrum source, the nature of the source is unclear. It might be a radio relic located in a galaxy cluster at $z \sim 0.6$.
-The relic in Abell 2048 and the source 24P73 are both classified as radio phoenices, which consist of compressed fossil radio plasma from AGNs. We detect several galaxies close to 24P73, probably belonging to the cluster hosting the radio phoenix.
-VLSS J0004.9−3457 is a diffuse radio source with emission surrounding the central elliptical galaxy of a small cluster or galaxy group. The source could be a radio mini-halo (or core-halo system). An arc-like structure is located to the east of the source which has a high polarization fraction of about 30% at 1.4 GHz indicative of ordered magnetic fields. This is probably a relic, where either particles are accelerated by the DSA mechanism or radio plasma from the central AGN is compressed.
-The origin of VLSS J0915.7+2511, a diffuse radio source in MaxBCG J138.91895+25.19876, is somewhat unclear. The source is most likely an AGN relic or radio phoenix.
We also presented optical images around five other diffuse radio source from the sample. For these sources, we could not find optical counterparts in POSS-II and 2MASS images. We detected candidate counterparts for all of these sources with redshifts in the range $0.5 < z < 1.2$. Some of these sources are radio galaxies, some others may be classified as mini-halos as the radio emission surrounds the host galaxy.

From our observations, we conclude that radio relics are located not only in the most massive merging galaxy clusters. They can also be found in smaller galaxy clusters and groups. Most of these sources probably trace old radio plasma from previous episodes of AGN activity. Several other sources resemble mini-halos or core-halos that are also found in less massive systems. Future low-frequency surveys will probably uncover large numbers of these sources, which can then be used to constrain timescales related to AGN activity and study the interaction between radio plasma and the ICM in clusters and galaxy groups.

Acknowledgements. We thank the staff of the GMRT who have made these observations possible. The GMRT is run by the National Centre for Radio Astrophysics of the Tata Institute of Fundamental Research.

The Westerbork Synthesis Radio Telescope is operated by ASTRON (Netherlands Institute for Radio Astronomy) with support from the Netherlands Foundation for Scientific Research (NWO). The National Radio Astronomy Observatory is a facility of the National Science Foundation operated under cooperative agreement by Associated Universities, Inc. The William Herschel Telescope and Isaac Newton Telescope are operated on the island of La Palma by the Isaac Newton Group in the Spanish Observatorio del Roque de los Muchachos of the Instituto de Astrofísica de Canarias.

This publication makes use of data products from the Two Micron All Sky Survey, which is a joint project of the University of Massachusetts and the Infrared Processing and Analysis Center/California Institute of Technology, funded by the National Aeronautics and Space Administration and the National Science Foundation. This research has made use of the VizieR catalogue access tool, CDS, Strasbourg, France.

The Digitized Sky Surveys were produced at the Space Telescope Science Institute under U.S. Government grant NAG W-2166. The images of these surveys are based on photographic data obtained using the Oschin Schmidt Telescope on Palomar Mountain and the UK Schmidt Telescope. The plates were processed into the present compressed digital form with the permission of these institutions. The Second Palomar Observatory Sky Survey (POSS-II) was made by the California Institute of Technology with funds from the National Science Foundation, the National Geographic Society, the Sloan Foundation, the Samuel Oschin Foundation, and the Eastman Kodak Corporation.

RJvW would like to thank S. van der Tol for helping with the observations. RJvW acknowledges funding from the Royal Netherlands Academy of Arts and Sciences.